Article

Allometric Scaling and Resource Limitations Model of Tree Heights: Part 2. Site Based Testing of the Model

Sungho Choi [1,*,†]**, Xiliang Ni** [1,2,†]**, Yuli Shi** [1,3]**, Sangram Ganguly** [4]**, Gong Zhang** [5]**, Hieu V. Duong** [6]**, Michael A. Lefsky** [6]**, Marc Simard** [7]**, Sassan S. Saatchi** [7]**, Shihyan Lee** [8]**, Wenge Ni-Meister** [8]**, Shilong Piao** [9]**, Chunxiang Cao** [2]**, Ramakrishna R. Nemani** [10] **and Ranga B. Myneni** [1]

[1] Department of Earth and Environment, Boston University, 675 Commonwealth Avenue, Boston, MA 02215, USA; E-Mail: ranga.myneni@gmail.com

[2] State Key Laboratory of Remote Sensing Sciences, Institute of Remote Sensing Applications, Chinese Academy of Sciences, Beijing 100101, China; E-Mails: nixl@irsa.ac.cn (X.N.); cao413@irsa.ac.cn (C.C.)

[3] School of Remote Sensing, Nanjing University of Information Science and Technology, Nanjing 210044, China; E-Mail: ylshi.nuist@gmail.com

[4] Bay Area Environmental Research Institute (BAERI)/NASA Ames Research Center, Moffett Field, CA 94035, USA; E-Mail: sangramganguly@gmail.com

[5] Department of Watershed Science, Utah State University, UT 84322, USA; E-Mail: gongzhang07@gmail.com

[6] Center for Ecological Analysis of Lidar, Natural Resource Ecology Laboratory, Colorado State University, Fort Collins, CO 80523, USA; E-Mails: Hieu.Duong@colostate.edu (H.D.); lefsky@cnr.colostate.edu (M.L.)

[7] Jet Propulsion Laboratory, California Institute of Technology, 4800 Oak Grove Dr., Pasadena, CA 91109, USA; E-Mails: marc.simard@jpl.nasa.gov (M.S.); saatchi@jpl.nasa.gov (S.S.)

[8] Department of Geography, Hunter College of CUNY, New York, NY 10065, USA; E-Mails: shihyanlee@yahoo.com (S.L.); Wenge.Ni-Meister@hunter.cuny.edu (W.N.)

[9] College of Urban and Environmental Sciences and Sino-French Institute for Earth System Science, Peking University, Beijing 100871, China; E-Mail: slpiao@pku.edu.cn

[10] Biospheric Science Branch, NASA Ames Research Center, Moffett Field, CA 94035, USA; E-Mail: rama.nemani@nasa.gov

† These authors contributed equally to this work.

* Author to whom correspondence should be addressed; E-Mail: schoi@bu.edu; Tel.: +1-617-353-8846; Fax: +1-617-353-8399.

Abstract: The ultimate goal of this multi-article series is to develop a methodology to generate continuous fields of tree height and biomass. The first paper demonstrated the need for Allometric Scaling and Resource Limitation (ASRL) model optimization and its ability to generate spatially continuous fields of tree heights over the continental USA at coarse (1 km) spatial resolution. The objective of this second paper is to provide an assessment of that approach at site scale, specifically at 12 FLUXNET sites where more accurate data are available. Estimates of tree heights from the Geoscience Laser Altimeter System (GLAS) waveform data are used for model optimization. Amongst the five possible GLAS metrics that are representative of tree heights, the best metric is selected based on how closely the metric resembles field-measured and Laser Vegetation Imaging Sensor tree heights. In the optimization process, three parameters of the ASRL model (area of single leaf, α; exponent for canopy radius, η; and root absorption efficiency, γ) are simultaneously adjusted to minimize the difference between model predictions and observations at the study sites (distances to valid GLAS footprints ≤ 10 km). Performance of the optimized ASRL model was evaluated through comparisons to the best GLAS metric of tree height using a two-fold cross validation approach (R^2 = 0.85; RMSE = 1.81 m) and a bootstrapping approach (R^2 = 0.66; RMSE = 2.60 m). The optimized model satisfactorily performed at the site scale, thus corroborating results presented in part one of this series. Future investigations will focus on generalizing these results and extending the model formulation using similar allometric concepts for the estimation of woody biomass.

Keywords: tree height; allometric scaling law; resource limitation; GLAS; model optimization

1. Introduction

Forest height and biomass are important attributes required for quantifying the dynamics of the terrestrial carbon cycle [1–4]. Several recent articles have reported variations in regional and global forest structural attributes [5] (e.g., under decreasing [6], increasing [7–9], or relatively steady-state [10] conditions), but there remains large uncertainty [11–13]. Two conventional methods of mapping tree heights and biomass are the extrapolation methods using field-measured and/or remote sensing altimetry data (e.g., regression tree or random forest algorithms [14–16]) and the physical/physiological model based on allometric scaling laws (e.g., Allometric Scaling and Resource Limitations (ASRL) model [17]).

The extrapolation methods well estimate forest structural attributes by exploiting advancements in remote sensing. Small footprint lidar, Terrestrial Laser Scanners [18,19] and Laser Vegetation Imaging

Sensor (LVIS) [20,21] are key to accurate estimation of tree heights and forest biomass. Global and regional maps of tree heights [14,15] and forest biomass [16,22,23] have been generated using lidar waveform data from the Geoscience Laser Altimeter System (GLAS) instrument onboard the Ice, Cloud and land Elevation Satellite (ICESat). The relatively large footprint and wide spatial coverage of the GLAS instrument have made large-scale mapping of forest heights feasible [24,25]. However, the physical/physiological mechanisms governing plant growth are often neglected in the extrapolation approaches. The ASRL model [17] alternatively uses allometric scaling rules, which relate tree heights and local energy budgets in the prediction of potential tree growth. Nevertheless, the premises of the ASRL model have an obvious limitation that the balance of internal flows (metabolic flow requirement, available flow, and evaporative flow) is independent of local landscape variations across different eco-climatic regimes and forest types of varying age classes, unlike a non-allometric scaling model (e.g., [26]). This results in disparities between observations and model predictions.

Therefore, the parametric optimization of the ASRL model possibly brings significant progress in mapping tree heights and biomass by incorporating actual observations (*i.e.*, GLAS waveform data) with the power of physical/physiological laws for scaling purpose. The feasibility of ASRL model optimization with high resolution remotely sensed altimetry data and its ability to predict tree heights are tested in the multi-article series with the ultimate goal of generating accurate spatially continuous fields of tree heights and biomass. Paper one in this series is focused on the application of the optimized ASRL model over the continental USA (CONUS) [27]. The forested lands in the CONUS were delineated into different eco-climatic zones based on dominant forest type, annual total precipitation amount and annual average temperature. The optimization involved finding the appropriate scaling parameters and exponents of the ASRL model in each of the eco-climatic zones using the Powell's optimization method [28]. A spatially continuous map of tree heights over the CONUS was satisfactorily reproduced in the first paper, but at coarse spatial scales (1 km). The objective of this second article is to test the methodology underlying these large-scale mapping efforts at finer spatial scales, *i.e.*, FLUXNET sites, where more accurate information is available. Future articles in this series will extend the allometric scaling and resource limitation concepts to estimation of woody biomass.

2. Data

2.1. Field Measurements

In this study, we used four different sources of field-measured tree heights. Data from 82 plots were assembled from seven field sites (Table 1) [20,21,29–35]. These data came from different measurement campaigns, or census, and are comprised of different acquisition dates with varying sizes and numbers of subplots as shown in Section S1 and Figure S1 of the Supplementary Material.

2.2. LVIS Data

LVIS is an airborne laser altimeter sensor that records the intensity of returned signals from a target surface [36]. An LVIS standard data product, *RH100*, was used in this study (Section S2.1). Lidar tree

heights could be influenced by topography and footprint size. Therefore, topographic effects were corrected from LVIS tree heights taking into account its footprint size (~20 m) [37].

LVIS datasets used in this study were categorized into two groups. The first dataset was used to compare LVIS heights with concurrent field-measured tree heights in seven different locations (Table 1 and Figure S1). In a separate exercise, the second dataset was used for comparisons between LVIS tree heights and GLAS height metrics. Except for the 2008 Sierra Nevada campaign, acquisition dates of the second dataset mostly overlapped with GLAS waveform acquisition dates (from 2003 to 2006; Table 2 and Figure S2).

Table 1. Datasets for inter-comparisons between field measured and Laser Vegetation Imaging Sensor (LVIS) waveform derived heights. There are 82 measurement plots spanning seven field sites in this study.

Sites	Field Measured Data				LVIS Data [38]
	Subplots	Acquisition Year	Plot Size (m)	References	Acquisition Year
La Selva Biological Station, Costa Rica	30	2006	10×100	[20,21]	2005
Barro Colorado Island, Panama	20	2000	100×100	[29–31]	1998
Penobscot Experimental Forest, Maine, USA	12	2009	50×200	[32,33]	2003
Sierra National Forest, California, USA	8	2008	100×100		2008
Harvard Forest, Massachusetts, USA	2	2007	100×100		2003
	2	2009	50×50		
Howland Research Forest, Maine, USA	2	2007	100×100	[34,35]	2003
	2	2009	50×50		
Bartlett Experimental Forest, New Hampshire, USA	2	2007	100×100		2003
	2	2009	50×50		

Table 2. Datasets for inter-comparisons between LVIS derived heights and Geoscience Laser Altimeter System (GLAS) height metrics (six different sites used in this study).
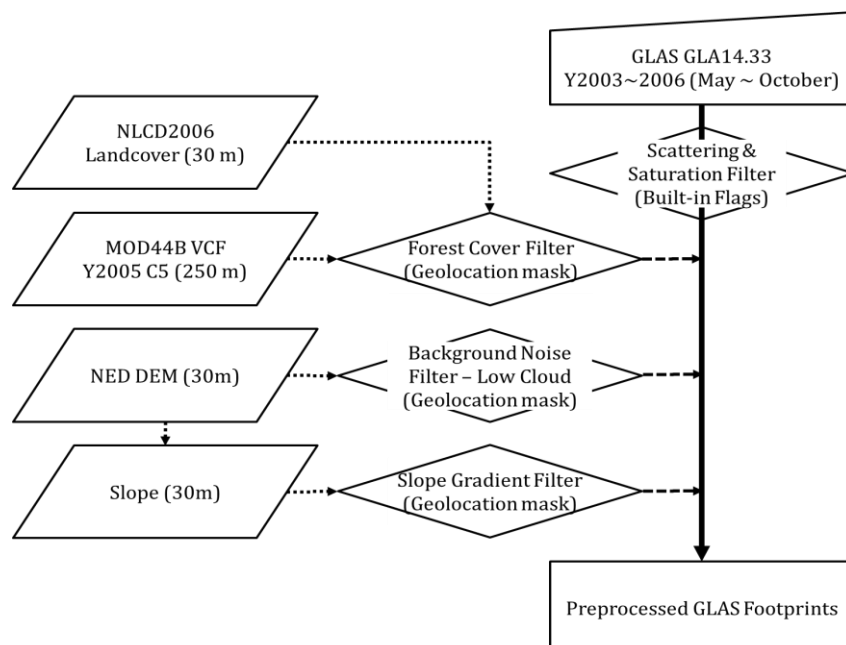
Sites	LVIS Data [38]	GLAS Data [39]
	Acquisition Year	
White River Wildlife Refuge, AR, USA	2006	2003–2006
Sierra Nevada, CA, USA	2008	2003–2006
Harvard Forest, MA, USA	2003	2003–2006
Patapsco Forest, MD, USA	2003	2003–2006
Howland Research Forest and Penobscot Experimental Forest, ME, USA	2003	2003–2006
Bartlett Experimental Forest, NH, USA	2003	2003–2006

2.3. GLAS Data

The latest release of GLAS laser altimetry data (Release 33) available from the National Snow and Ice Data Center was used in this study. GLAS waveform data provide information on land elevation and vegetation cover within its ellipsoidal footprints at ~170 m spaced intervals [40,41]. We used GLAS Level-2 Land Surface Altimetry (GLA14) product, which includes geolocation of footprints and waveform parameters such as signal beginning and echo energy peaks [40]. It is difficult to estimate the dimension and shape of every single GLAS footprint. Therefore, all GLAS footprints were assumed to have a circular diameter of 70 m [42] in this study.

Figure 1 depicts the sequential preprocessing/filtering steps for selecting valid GLAS waveforms. Data from May to October of each year were considered, as this period best approximates the growing season. GLAS data were further screened by applying several preprocessing filters, such as atmospheric forward scattering and signal saturation, background noise level correction and landcover mask conditions (Section S2.2, S2.3, S3, and Figure S3 for preprocessing datasets). GLAS footprints have a coarser spatial resolution (70 m) than some preprocessing datasets (e.g., National Land Cover Database is at 30 m spatial resolution). A GLAS footprint is possibly located over heterogeneous forest types and topographic conditions. This study used preprocessing data values of nearest pixels to the center of a GLAS footprint as the normalized lidar intensity of GLAS data peaks at the center of footprint [37].

Figure 1. Preprocessing/filtering steps for determining valid GLAS waveform data. Ancillary datasets required include National Land Cover Database (NLCD) Landcover, Moderate Resolution Imaging Spectroradiometer (MODIS) Vegetation Continuous Fields (VCF) and National Elevation Dataset (NED)-derived Digital Elevation Model (DEM).
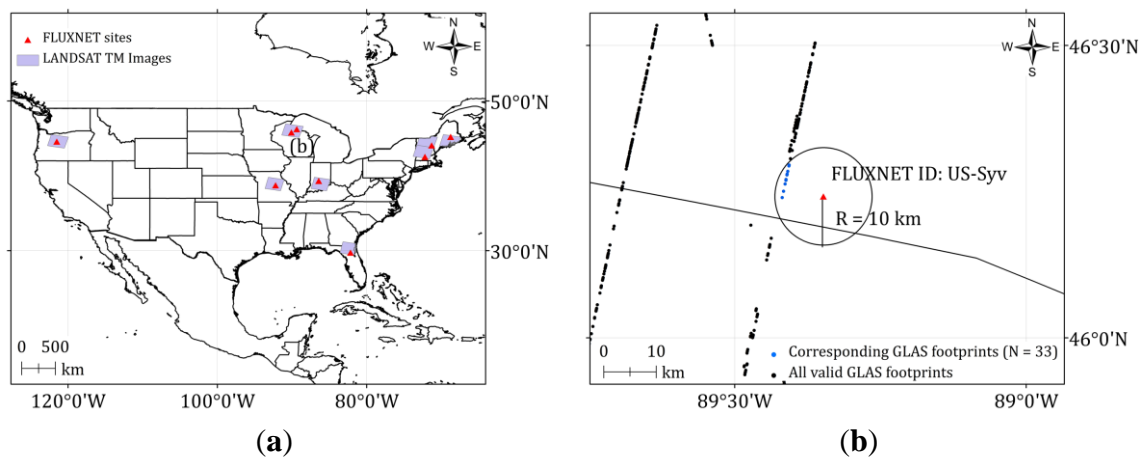

2.4. Input Data for the ASRL Model

The ASRL model predicts potential tree heights. The model combines statistical allometric scaling laws with local energy budgets constrained by resource limitations such as water, radiation, wind and air temperature [17]. The model is driven by input climatic variables and tree trait parameters. Input

climatic variables are annual incoming solar radiation, annual total precipitation, annual average temperature, annual average wind speed and annual average relative humidity. Additionally, Leaf Area Index (LAI) and Digital Elevation Model (DEM) are required for initializing the model. Table S1 lists the input datasets (climatic and ancillary data).

2.4.1. FLUXNET Data

The analysis in this paper is focused on sites from the FLUXNET network [43]. We chose 12 sites, amongst the 71 sites over the CONUS, based on distance between a site and valid GLAS footprints (≤10 km radius; Figure 2 and Table 3). Annual total precipitation and annual average temperature data (from 2001 to 2006) were obtained from the selected sites.

> **Figure 2.** (**a**) The 12 selected FLUXNET sites (red triangles) based on the distance from valid GLAS footprints (≤ 10 km radius). (**b**) An example site (ID: US-Syv) located at the Sylvania Wilderness Area of Michigan. Purple polygons represent Landsat TM imagery for the retrieval of Leaf Area Index (LAI). Blue dots refer to valid GLAS footprints corresponding to the FLUXNET site.

(**a**)   (**b**)

2.4.2. DAYMET Data

The FLUXNET datasets do not contain all the input climatic variables required by the ASRL model. Annual incoming solar radiation, annual average wind speed and annual average vapor pressure were therefore obtained from the DAYMET database [44] at a spatial resolution of 1 km. DAYMET climatic values were extracted from pixels nearest to our study sites. Annual vapor pressure was converted into annual relative humidity using a formula provided by the World Meteorological Organization (WMO) [45].

2.4.3. Ancillary Data for the ASRL Model (LAI and DEM)

The ASRL model requires two ancillary variables: (a) LAI and (b) DEM. Several Landsat TM scenes (Figure 2(a)) were obtained for the period 2003 to 2006 with near-similar acquisition dates (June to September) as the GLAS waveform data. The Landsat Ecosystem Disturbance Adaptive Processing System [46] and a physically-based algorithm [47] were used to retrieve LAI values. As

with the DAYMET data, we extracted LAI and DEM values of the pixels nearest to the study sites. Neighboring pixels in a 3 × 3 window showed minimal variability in both LAI and DEM at 30 m spatial resolution (absolute variation coefficients <5%).

Table 3. The 12 FLUXNET sites selected for analysis in this study based on the distance between a site and valid GLAS footprints (≤10 km radius). The three dominant forest types at these sites are Evergreen Needleleaf Forest (ENF), Deciduous Broadleaf Forest (DBF), and Mixed Forests (MF). Percent tree cover values were derived from the MODIS VCF product.

FLUXNET SITE ID	Site Name	Location	Temporal Range of Data	Forest Types	% Tree Cover	Valid GLAS Footprints
US-Me1	Metolius Eyerly Burn	OR, USA	2004–2005	ENF	63	29
US-Syv	Sylvania Wilderness Area	MI, USA	2001–2006	MF	52	33
US-Ha1	Harvard Forest EMS Tower	MA, USA	1992–2006	DBF	74	68
US-Ho1	Howland Forest (main tower)	ME, USA	1996–2004	ENF	73	33
US-MMS	Morgan Monroe State Forest	IN, USA	1999–2006	DBF	70	18
US-Bar	Bartlett Experimental Forest	NH, USA	2004–2006	DBF	93	12
US-Ha2	Harvard Forest Hemlock Site	MA, USA	2004	ENF	74	67
US-MOz	Missouri Ozark Site	MO, USA	2004–2007	DBF	51	64
US-Ho2	Howland Forest (west tower)	ME, USA	1999–2004	ENF	74	31
US-LPH	Little Prospect Hill	MA, USA	2003–2005	DBF	73	68
US-SP3	Slashpine-Donaldson-mid-rot-12yrs	FL, USA	2008	ENF	51	30
US-WCr	Willow Creek	WI, USA	1999–2006	DBF	51	9

3. Methods

3.1. GLAS Metric Selection

Prior to the optimization of the ASRL model with GLAS tree heights, we perform an exercise finding the best GLAS metric that closely corresponds to field-measured and LVIS derived tree heights. This analysis is based on two premises: (a) canopy height derived from LVIS data is related to field-measured tree height as reported in previous studies [2,37,48–50] and (b) the best GLAS metric, inferred from comparison of five GLAS metrics with LVIS tree heights, improves model optimization. Several recent articles have evaluated GLAS tree heights directly with field data [14,51–53] and/or with airborne lidar data [37,54–56].

The root mean square error (RMSE) and R^2 (from the linear-regression) are used to determine how well tree heights are related to each other in the inter-comparisons among field-measured, LVIS, and GLAS derived tree heights. Systematic errors related to biases in measurements are additionally considered in the interpretation of results.

3.1.1. Comparison between Field-Measured and LVIS Tree Heights

Field-measured datasets used in this study differed in their sampling methodologies and plot designs. Also, the coordinates of individual trees were not recorded in every measurement campaign/census. This precluded a footprint-level comparison between field-measured and LVIS tree

heights, unlike in some previous studies [2,48]. Therefore, we performed comparisons at the plot-level by calculating representative tree height values from field measurements and LVIS data, which were defined as the average of the top 25% tree heights in each of the subplots (e.g., Figure S4). This approach minimizes overestimations (e.g., using only three highest values [37]) or underestimations (e.g., using all values [2]) if there are large numbers of field-measured trees and LVIS footprints in a subplot. The RMSE is calculated using Equation 1.

$$RMSE_{field\,vs.\,LVIS} = \sqrt{\frac{\sum_{i=1}^{n}\left(\overline{H}_{field\,measured,i} - \overline{H}_{LVIS,i}\right)^2}{n}} \qquad (1)$$

here $H_{field\text{-}measured}$ is the mean height of top 25% of field-measured trees in a subplot, H_{LVIS} refers to the mean value of top 25% LVIS tree heights in the same subplot and i corresponds to the sample subplot ($n = 82$) as shown in Table 1.

3.1.2. Comparison between LVIS Tree Heights and GLAS Height Metrics

Three standard altimetry variables are available from the GLA14 product based on the Gaussian decomposition approach [57]: (a) signal begin range increment, *SigBegOff*, (b) signal end range increment, *SigEndOff* and (c) centroid range increment for the last Gaussian Peak, *gpCntRngOff 1*. Theoretically, *gpCntRngOff 1* and *SigEndOff* are assumed to represent the ground level elevation within a GLAS field-of-view, while *SigBegOff* refers to the highest point of a surface. In practice, *(SigBegOff − SigEndOff)* and *(SigBegOff − gpCntRngOff 1)* may not be identical due to topographic and roughness effects [37]. There are five possible GLAS metrics representative of tree heights based on the Gaussian decomposition approach and topographic effect correction (H_{A-E} in Table 4 and Section S4).

Table 4. Five possible GLAS height metrics based on Gaussian decomposition approach and topographic effect correction. Statistical analysis examining the full GLAS waveform extents [24,55,58,59] is beyond the scope of this study.

GLAS Height Metrics	Applied GLAS Waveform Parameters	Topographic Effect Correction	References
H_A	*SigBegOff − gpCntRngOff 1*	No	[22,51,60]
H_B	SigBegOff − *SigEndOff*	No	[52]
H_C	*SigBegOff − gpCntRngOff 1*	Yes	[14,37,56]
H_D	*SigBegOff − SigEndOff*	Yes	-
H_E	*SigBegOff − 2 × gpCntRngOff 1 + SigEndOff*	No	-

The spatial correspondence between LVIS and GLAS footprints was determined using the maximum distance from the center of a GLAS footprint to any LVIS footprint (within ~45 m;

Figure S5). The RMSEs between LVIS heights and five possible GLAS height metrics were obtained from Equation (2):

$$RMSE_{A-E} = \sqrt{\frac{\sum_{i=1}^{n_{A-E}}\left(H_{GLAS:A-E,i} - \overline{H}_{LVIS,i}\right)^2}{n_{A-E}}}$$ (2)

here H_{LVIS} is the mean value of top 25% of LVIS heights within a GLAS footprint, H_{GLAS} is GLAS tree heights, A–E refers to the five possible GLAS height metrics (Table 4), and i represents the sample GLAS footprint ($n = 133$).

The result analyses were stratified into three groups, based on topographic conditions over the GLAS footprint, as low (slope $\leq$ 5 °), intermediate (5 °$<$ slope $\leq$ 10 °) and high (10 °$<$ slope $\leq$ 20 °). All outliers were removed in this comparison exercise, *i.e.*, only GLAS tree heights within two standard deviations from the mean height were considered (~95%; 5 m $< H_{A-E} \leq$ 100 m).

3.2. ASRL Model Optimization

3.2.1. Initial ASRL Model Predictions (Potential Tree Heights)

The initial model runs are driven by input datasets and result in potential tree heights at each study site. Key climate input data (temperature and precipitation) are derived from FLUXNET sites. DAYMET, LAI, and DEM grids nearest to the study sites provide other climatic variables and ancillary data for the model runs. The unoptimized ASRL model predicts only potential tree heights considering hydraulic limits to tree growth. These differ from observations due to the fact that the unoptimized model applies homogeneous steady-state allometric scaling laws across different environmental conditions and forest types with varying age classes [27].
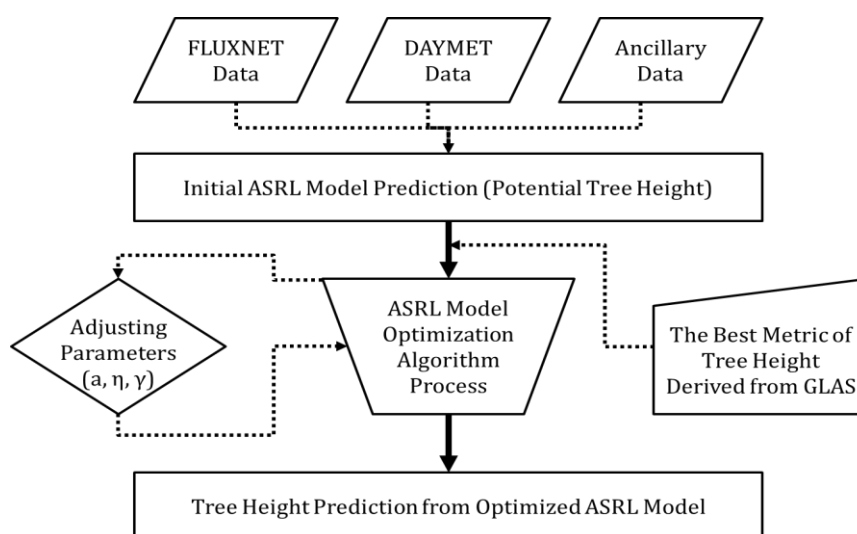
3.2.2. Optimized ASRL Model Predictions

Remote sensing based altimetry data, which provide actual tree heights, can alleviate the limitation of the unoptimized ASRL model related to different growing conditions and forest types with varying age classes. The model optimization is detailed in the first paper of this series [27]. Model optimization is aimed at minimizing the difference between GLAS tree heights and model predictions (Figure 3) based on the Powell's optimization methodology [28]. A merit function was formulated and implemented from Press *et al.* [61] and Kuusk and Nilson [62]. It finds the maximum likelihood estimates of each parameter that result in minimizing the merit function. Amongst the five GLAS height metrics, the model optimization uses the best GLAS metric that is closest to the field-measured and LVIS tree heights.

Three model parameters are iteratively adjusted during optimization: (a) area of single leaf, α, (b) exponent for canopy radius, η, and (c) root absorption efficiency, γ. The respective initial values are 13 cm^2, 1.14, and 0.33 [17]. α is related to the collection of solar radiation for plant growth, and it is used to calculate the coefficients for canopy transmissions. In the ASRL model, energy budget in a single leaf is accumulated to a canopy-level budget [17]. The geometry of canopy is associated with η controlling the scaling of canopy radius with tree height. This derives the rate of absorbed solar

radiation in the ASRL model [17]. γ determines the available flow rate given the incoming rate of precipitation within the root capture area. Local γ varies depending on soil type and hydrology [17]. To achieve convergence, the following ranges were used: $1 \text{ cm}^2 \leq \alpha < 100 \text{ cm}^2$, $0.8 \leq \eta < 1.5$, and $0.1 \leq \gamma < 0.8$ (as in the TRY database [63]). Kempes *et al.* [17] tested η and γ individually in a sensitivity analysis. This study added α to the optimization scheme because the area of a leaf significantly varies across different eco-climatic regimes and forest types [64,65]. Also, α is an important parameter determining net radiation and fluxes of sensible and latent heat (e.g., [66]).

Figure 3. Diagram showing ASRL model optimization. The model predicts potential tree heights (initial prediction) using climatic and ancillary data. Three allometric scaling parameters of the model (area of single leaf, α; exponent for canopy radius, η; and root absorption efficiency, γ) are simultaneously adjusted to find the minimum of the difference between GLAS tree heights and model predictions. GLAS tree heights are estimated using the best GLAS metric that closely resembles field-measured and LVIS tree heights amongst five GLAS height metrics (Table 4).

Our approach has constraints due to a limited number of scaling parameters (α, η, and γ) explored in the model optimization and an assumption that allometric scaling laws at individual tree level are applicable at larger scales. In addition, a limitation of this study is that the model does not directly account for variation in forest stand age in the optimization process. Tree heights and growth rates are clearly related to forest stand ages [67,68], varying across different forest types and growing conditions. However, it does not necessarily mean that our methodology neglects forest stand ages in the estimation of tree heights. GLAS waveform data indirectly brings age information of forests into the ASRL model for the parametric optimization, as actual heights are associated with forest stand ages.

3.3. Evaluation of the Optimized ASRL Model Predictions

3.3.1. Two-Fold Cross Validation Approach

The performance of the optimized ASRL model is evaluated through comparisons against GLAS tree heights in this study. The two-fold cross validation technique is a common statistical approach that

randomly divides original samples into two equal sets of training and test data. The first half of GLAS tree heights was used as a training dataset to optimize the model at a site. The test dataset was prepared by averaging the remaining half of GLAS tree heights at the same site. Training and test GLAS data are completely separated in the cross validation (*i.e.*, no overlapping each other). The RMSE is estimated to interpret the relationship between GLAS tree heights and optimized model predictions (Equation (3)) along with R^2 from the linear regression.

$$RMSE_{ASRL\,I} = \sqrt{\frac{\sum_{i=1}^{n}\left(\overline{H}_{GLAS\,test,\,i} - H_{opt\,ASRL\,training,\,i}\right)^2}{n}} \qquad (3)$$

here $H_{opt\,ASRL\,training}$ is the optimized model prediction using the GLAS training data at a site, $H_{GLAS\,test}$ represents the mean of tree heights computed from the GLAS test data at the same site, and i refers to the site ($n = 12$).

3.3.2. Bootstrapping Approach

A second evaluation of the optimized ASRL model was performed at the eco-climatic zone scale [27]. Individual FLUXNET sites were grouped into eco-climatic zones (Figure S6). Each zone consisted of 1 to 2 FLUXNET sites at the most. We neglected zones where GLAS footprints were less than 50 based on the need for model optimization. Selected sites include Harvard Forest EMS Tower (US-Ha1), Howland Forest Main Tower (US-Ho1), Howland Forest West Tower (US-Ho2), Harvard Forest Hemlock Site (US-Ha2), Missouri Ozark Site (US-MOz), and Little Prospect Hill (US-LPH) within a total of five eco-climatic zones (Table S2).

A bootstrapping approach [69] was applied to evaluate the optimized model predictions for the five zones. Corresponding GLAS footprints were randomly divided into two groups (training and test datasets). The bootstrapping generated extra comparison sets (subsamples, N = 100) to examine the stability of the results. Training subsamples of the GLAS tree heights were used for model optimization. The optimized ASRL model predictions were then compared to the average of tree heights derived from test subsamples by calculating the RMSE (Equation 4). R^2 from the linear regression is additionally provided for the interpretation. Two groups of subsamples (training and test) also have no overlaps in each other.

$$RMSE_{ASRL\,II} = \sqrt{\frac{\sum_{i=1}^{n}\sum_{j=1}^{100}\left(\overline{H}_{GLAS\,test,\,i,\,j} - H_{opt\,ASRL\,training,\,i,\,j}\right)^2}{n}} \qquad (4)$$
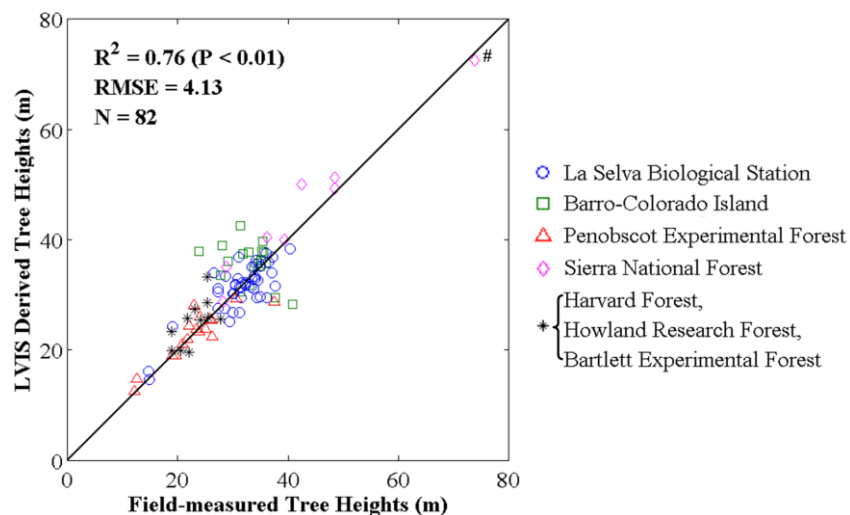
here $H_{opt\,ASRL\,training}$ is the optimized model prediction using bootstrapping subsamples of training GLAS waveform data for a zone, $H_{GLAS\,test}$ represents the mean of tree heights derived from test GLAS subsamples within the same zone, i refers to the sample eco-climatic zone ($n = 5$), and j corresponds to the bootstrapping subsample (a total of 100 sets for a climatic zone).

4. Results and Discussion

4.1. Best GLAS Height Metric from Inter-Comparisons with Field-Measured and LVIS Tree Heights

We first performed a plot-level comparison between LVIS tree heights and field measurements (Figure 4). The statistical significance of this relationship (R^2 = 0.76 and RMSE = 4.13 m) is comparable to previous reports (footprint-level comparison [50] and plot-level comparison [37]). Some disagreements are due to differences in data acquisition times. For example, field measurements for the Penobscot Experimental Forest (Maine, USA) were conducted in 2009, while the LVIS data were acquired in 2003. Similarly, the LVIS acquisition date is six years prior to field measurements of the 2009 New England Campaign (Table 1).

> **Figure 4.** Comparison of LVIS tree heights with field measurements. A total of 82 plots from seven different sites are considered in this analysis. Regression analysis indicates a statistically significant relationship between LVIS tree heights and field measurements ($p < 0.01$). [#] In Sierra National Forest, there is one extremely influential observation due to old growth forests (ages > 150; [70]).

The average tree growth rates in study regions can be approximated using an equation of Shugart *et al.* [67]. The map of forest age distribution in North America [70] shows that forest stands are aged from 41 to 80 in New England (Maine, Massachusetts, and New Hampshire). We expect that tree growths in New England can be made roughly up to 1.3 m for 6 years.

Relatively large deviation is found in the results of Barro-Colorado Island. Two plausible reasons are associated with (a) tree growth rates of tropical forest and (b) terrain features and densely vegetated environment of the study area. Tropical forests increase more in size [71] compared to USA forests for a similar period. This explains that field measured tree heights (year 2000) are larger than LVIS tree heights (year 1998). Another plausible reason for disagreements is that the LVIS is a large-footprint lidar (20 m), which is significantly affected by the topography and denseness of vegetation over the ground [72]. Especially, Barro Colorado Island consists of dense tropical forest and some plots are located over steep terrains. This possibly decreases the measurement accuracy of LVIS data, inflating deviations.

Subsequent analysis was focused on comparison of five metrics derived from GLAS waveform data (H_{A-E}; Table 4) with LVIS tree heights, at six sites with terrain slope condition $\leq 5°$ (Figure 5). Results for other slope categories are shown in Figure S7 and S8. We observed an overestimation of GLAS tree heights relative to LVIS tree heights, similar to previous studies [37,56]. Among the five GLAS height metrics, H_C was best correlated to LVIS tree heights (R^2 of 0.70 and RMSE of 4.42 m ($P < 0.01$)). This metric was derived from the distance between the last Gaussian peak and signal beginning of the GLAS waveform and incorporated topographic effect correction. Overestimations are related to both topographic gradient effects and GLAS waveform parameters. The bias increased with increasing tree heights (H_A and H_B; Figure 5(a,b)), as previously noted in Lee *et al.* [37]. Also, significant biases were generated for taller trees from use of the full GLAS waveform extents (H_B and H_D; Figure 5(b,d)). As shown in Figures 5e, a relatively low correlation with LVIS tree heights was obtained from the metric using all three GLAS waveform parameters (*i.e.*, signal begin, end, and the last Gaussian peak).

Similarly, for regions with intermediate slope condition (Figure S7) H_C was best correlated with LVIS tree height but with a lower R^2 and larger RMSE as compared to the low slope condition. In the case of high topographic gradients (Figure S8), H_D showed better correspondence with LVIS heights, however, the correlations were significantly lower for all five metrics.

Figure 5. Comparison of five GLAS-derived metrics (**a–e**, H_{A-E}; Table 4) with LVIS tree heights. The slope of the terrain in all cases is less than or equal to 5°. Comparisons for other topographic conditions (slope > 5°) are shown in Figure S7 and S8.
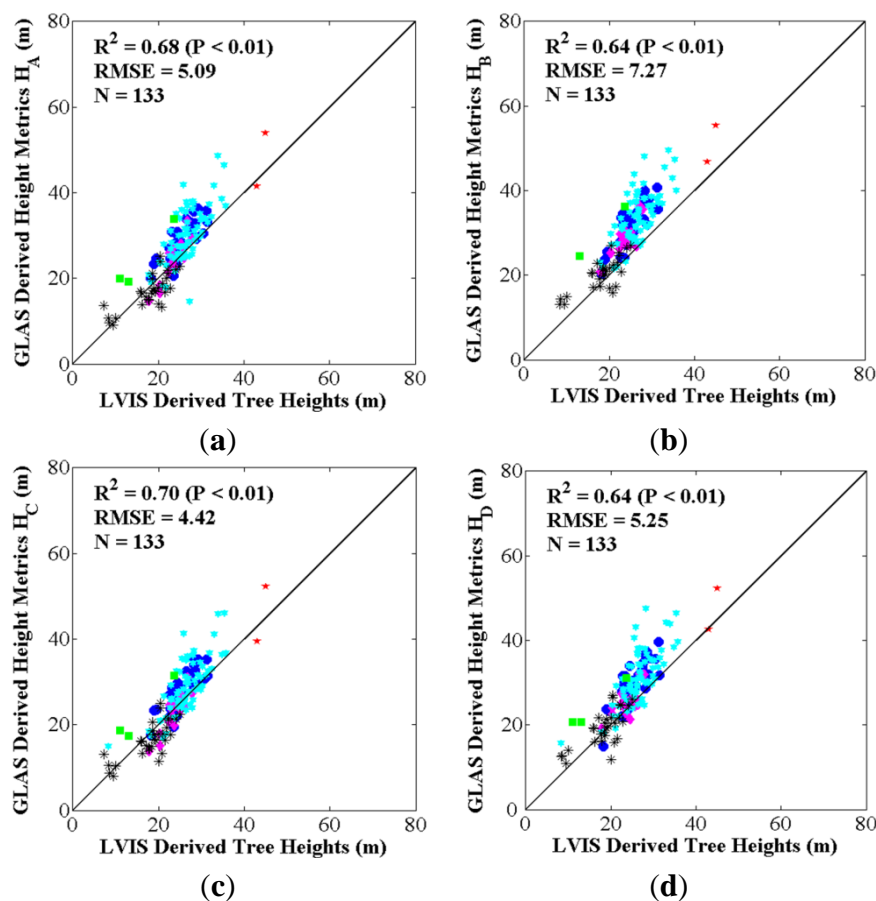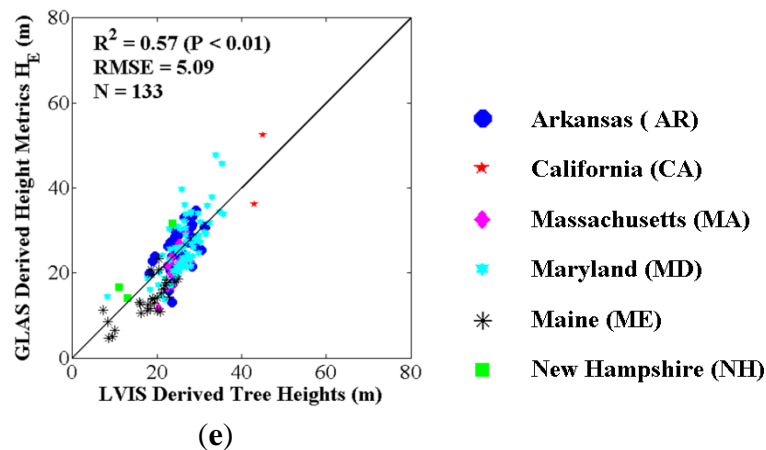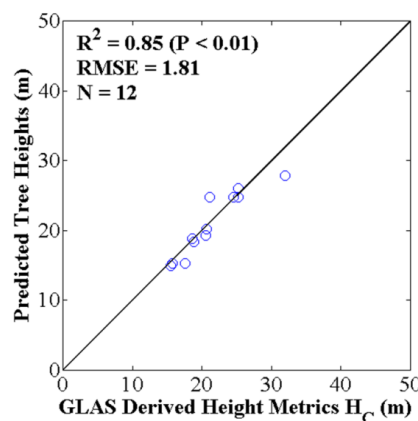
Figure 5. *Cont.*

(**e**)

4.2. Optimized ASRL Model Predictions and Evaluations

The ASRL model was optimized using tree heights derived from the best GLAS height metric (*i.e.*, H_C; Section 4.1) for all the 12 FLUXNET sites. The number of sample GLAS tree heights in the two-fold cross validation varied from 5 to 34 depending on the site (Table S3). A statistically significant relationship ($R^2 = 0.85$; RMSE = 1.81 m; $P < 0.01$) was obtained when comparing the optimized model predictions with the average of test GLAS tree heights (Figure 6). Kempes *et al.* [17] similarly tested the adjustment of individual allometric parameters of the ASRL model (e.g., stomatal density and root absorption efficiency) but reported less variation in model errors from the sensitivity analysis.

> **Figure 6.** Comparison of the optimized ASRL model predictions with the best GLAS
> metric of tree height (H_C in Figure 5(c)) at the FLUXNET sites (N = 12). We used a
> two-fold cross validation approach that randomly divides GLAS tree heights into two equal
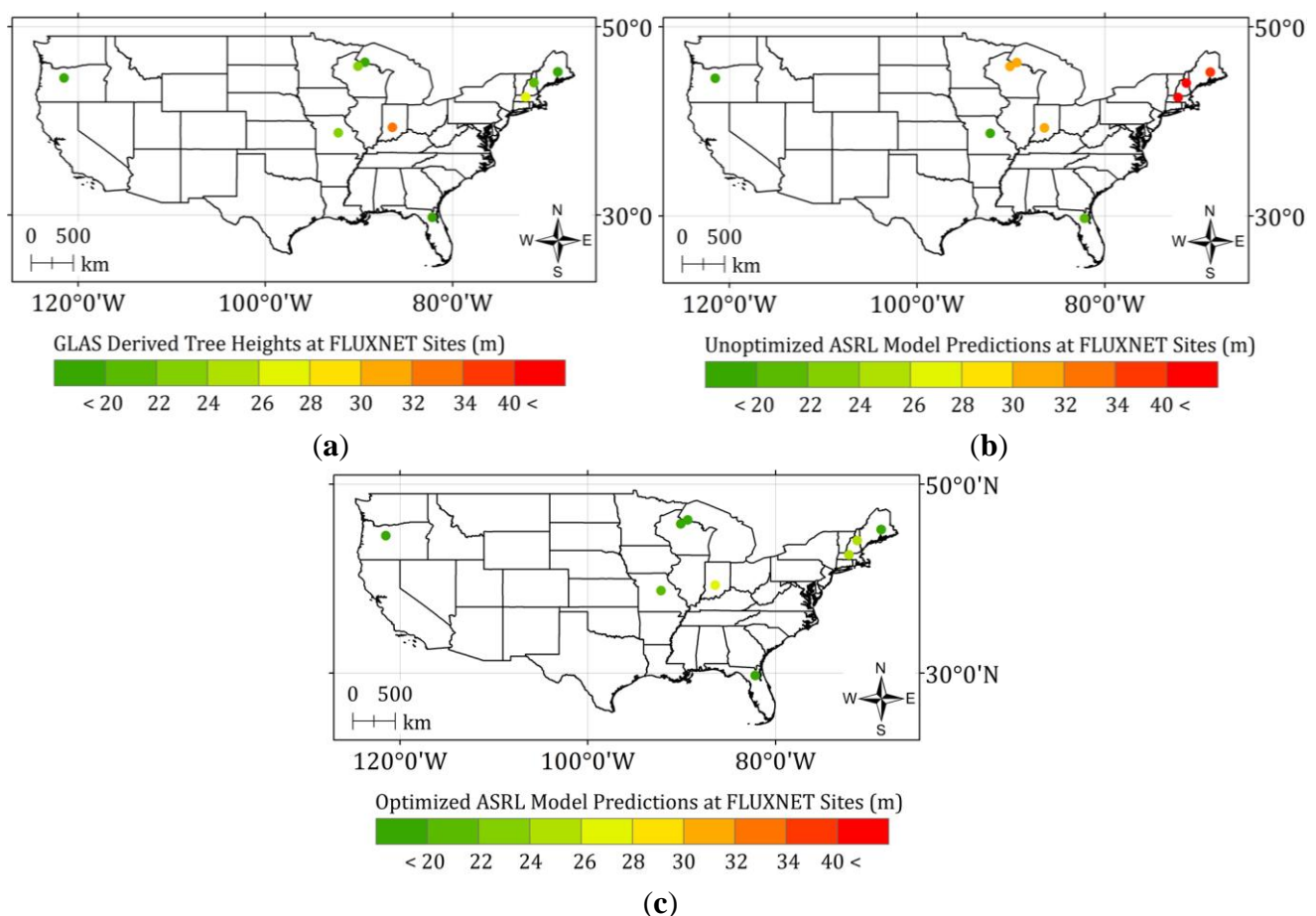> sets of training and test data.

The optimized values of allometric parameters for the study sites are listed in Table S3. There were notable adjustments in the optimized values of leaf size, α (initial value: 13.0 cm^2). It varied from 14.0 cm^2 for the US-MMS site to 56.0 cm^2 for the US-Ha2 site. This supports the relative significance of selecting α as an additional allometric parameter in model optimization. The other two allometric

parameters, exponent for canopy radius, η (initial value: 1.14) and root absorption efficiency, γ (initial value: 0.33), were also adjusted in the optimization with η values ranging from 0.94 for the US-MOz site to 1.24 for the US-Ha1 site and γ ranging from 0.19 for the US-Ho1 site to 0.38 for the US-SP3 site. These parameters were relatively stable compared to α, as previously reported by Kempes *et al.* [17].

Optimizing three parameters clearly improved model performance. Figure 7 shows the distribution of tree heights over 12 FLUXNET sites. Compared to the unoptimized ASRL model predictions (Figure 7(b)), tree heights from the optimized ASRL model (Figure 7(c)) better resemble GLAS tree heights (Figure 7(a)). As shown in Figure S9, the variance of model errors to the actual observation, "(*GLAS tree heights—Predicted tree heights*)/*GLAS tree heights*" [17], decreased from 0.53 (without optimization) to 0.01 (after optimization).
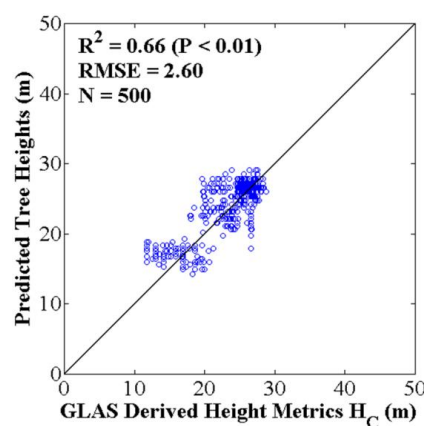
We performed a second evaluation of the optimized ASRL model at the eco-climatic zone scale (Table S2). Cold and drier regions are characterized by the zone ID 2, while zone ID 1, 3 and 5 represent cold and wetter regions. Zone ID 4 is located in the relatively warm and dry region. This definition of eco-climatic zones is comparable to the traditional eco-climatic zones (e.g., Holdridge life zones [73])—zone ID 1, 3 and 5 are related to the *Cool Temperate Wet Forest*, while ID 2 and 4 represent the *Cool Temperate Moist Forest* and *Warm Temperate Dry Forest*, respectively.

Figure 7. Distributions of tree heights over 12 FLUXNET sites: (**a**) GLAS tree heights, (**b**) unoptimized ASRL model predictions, and (**c**) optimized ASRL model predictions using training GLAS tree heights (two-fold cross validation).

(**a**)

(**b**)

(**c**)

As shown by the bootstrapping evaluation approach (Figure 8), the optimized model satisfactorily predicted tree heights (R^2 = 0.66; RMSE = 2.60 m; P < 0.01). The model's error variance decreased from 0.60 to 0.02 after optimization (Figure S10). Overall, the optimization successfully alleviated the effect of different environmental conditions and forest types and thus generated a more robust prediction of tree heights at a local scale, as indicated by the results of the two evaluation approaches. However, our approach did not consider the error propagation related to uncertainties in such input climatic variables and the GLAS waveform data, which are critical inputs to the optimized ASRL model. Input climate data may have produced large uncertainties due to the interpolation of climatic variables that are sensitive to terrain conditions (e.g., [74,75]). Model predictions and evaluations carry certain constraints that GLAS tree heights are taken as true values of tree heights in spite of inherent uncertainties in GLAS waveform data: topographic effects [55] might not be completely corrected from GLAS data. In addition, GLAS undersampling for some of the climatic zones results in fewer comparison sets in the optimization process, that is, increasing uncertainties.

Figure 8. Bootstrapping evaluation of the optimized ASRL model. The optimized model used the best GLAS tree height metric (H_C in Figure 5(c)). 100 sets of bootstrapping subsamples were generated for five eco-climatic zones.

5. Concluding Remarks

The Allometric Scaling and Resource Limitations (ASRL) model optimized with the Geoscience Laser Altimeter System (GLAS) waveform data was tested at site scale (12 FLUXNET sites over the continental USA) in this second of a multi-article series. The model predicts potential tree heights based on local energy budgets limited by water, radiation, wind and air temperature. Predicted potential tree heights differ from observations due to homogeneous scaling parameters and exponents across different eco-climatic zones and forest types with varying age classes. Model optimization in this study is aimed at minimizing the difference between model predictions and observations (*i.e.*, GLAS tree heights). This study considered three allometric parameters (area of single leaf, α; exponent for canopy radius, η; and root absorption efficiency, γ) for model optimization.

Amongst the five GLAS metrics (H_{A-E}) indicative of tree heights, the best GLAS metric (H_C) was used in model optimization. We conducted comparisons showing the closeness between: (a) Laser Vegetation Imaging Sensor (LVIS) tree heights and field measurements (R^2 = 0.76; RMSE = 4.13 m) and (b) the five GLAS metrics of tree heights and LVIS tree heights (R^2 = 0.70; RMSE = 4.42 m for

H_C). This best GLAS metric (H_C) was retrieved from the distance between the last Gaussian peak and signal beginning of the GLAS waveform and incorporated topographic effect correction.

The optimized model prediction was evaluated using two-fold cross validation and bootstrapping exercises. Predicted tree heights explained 85% of the variability in GLAS tree heights and on average showed an estimation error of 1.81 units of height from the two-fold cross validation approach at the studied sites. The variance of model errors to observation decreased from 0.53 to 0.01 after model optimization. In the case of bootstrapping, the study sites were stratified into five eco-climatic zones based on dominant forest type, annual total precipitation and annual average temperature. This exercise also resulted in a satisfactory prediction of GLAS tree heights by the optimized model ($R^2 = 0.66$; RMSE = 2.60 m) and a decrease in model error variance from 0.60 to 0.02 after optimization.

This investigation at site scale provides evidence corroborating our initial study [27] to the need for optimization and utility of the ASRL model with the ultimate goal of generating spatially continuous maps of tree heights and biomass. Optimization with remote sensing altimetry data successfully takes into account the external effect imposed by different eco-climatic regimes and forest types. The ASRL model was clearly improved by the parametric optimization showing the potential of the model in mapping tree heights. Nevertheless, the results from this site-specific analysis cannot be generalized due to the limited number of study sites and available GLAS waveform data. The studied sites did not cover the full range of precipitation, temperature and forest types prevalent across the continental USA. The optimized ASRL model has certain limitations due to (a) uncertainties of input climate and GLAS data and (b) a limited number of parameters explored in the optimization. Also, forest stand ages were not directly involved in the model optimization.

Forthcoming investigations will focus on extending the model formulation using similar concepts for the estimation of woody biomass (next two articles in preparation). Also, our approach will be tested over different study locations (e.g., China and Amazon Basin) to generalize the results for mapping global tree heights and biomass. A future research will be conducted over Amazon Basin where eco-climatic regimes and forest types are quite different from the CONUS. The availability of input climate data with good quality is certainly a challenge in this study region. Additionally, eco-climatic regimes and forest types of some regions in China may resemble those of the CONUS, but scaling parameters of the ASRL model are not necessarily identical. Hence, we will investigate the feasibility of the ASRL model in various regions by obtaining the appropriate scaling parameters.

Acknowledgments

References

1. Clark, D.B.; Clark, D.A. Landscape-scale variation in forest structure and biomass in a tropical rain forest. *Forest Ecol. Manage.* **2000**, *137*, 185–198.
2. Drake, J.B.; Dubayah, R.O.; Clark, D.B.; Knox, R.G.; Blair, J.B.; Hofton, M.A.; Chazdon, R.L.; Weishampel, J.F.; Prince, S.D. Estimation of tropical forest structural characteristics using large-footprint lidar. *Remote Sens. Environ.* **2002**, *79*, 305–319.

3. Muraoka, H.; Koizumi, H. Satellite Ecology (SATECO)-linking ecology, remote sensing and micrometeorology, from plot to regional scale, for the study of ecosystem structure and function. *J. Plant Res.* **2009**, *122*, 3–20.

4. Laumonier, Y.; Edin, A.; Kanninen, M.; Munandar, A.W. Landscape-scale variation in the structure and biomass of the hill dipterocarp forest of Sumatra: Implications for carbon stock assessments. *Forest Ecol. Manage.* **2010**, *259*, 505–513.

5. Rautiainen, A.; Wernick, I.; Waggoner, P.E.; Ausubel, J.H.; Kauppi, P.E. A National and international analysis of changing forest density. *Plos One* **2011**, *6*, doi: 10.1371/journal.pone.0019577.

6. Gonzalez, P.; Tucker, C.J.; Sy, H. Tree density and species decline in the African Sahel attributable to climate. *J. Arid Environ.* **2012**, *78*, 55–64.

7. Liski, J.; Korotkov, A.V.; Prins, C.F.L.; Karjalainen, T.; Victor, D.G.; Kauppi, P.E. Increased carbon sink in temperate and boreal forests. *Climatic Change* **2003**, *61*, 89–99.

8. Kauppi, P.E.; Rautiainen, A.; Korhonen, K.T.; Lehtonen, A.; Liski, J.; Nojd, P.; Tuominen, S.; Haakana, M.; Virtanen, T. Changing stock of biomass carbon in a boreal forest over 93 years. *Forest Ecol. Manage.* **2010**, *259*, 1239–1244.

9. Rautiainen, A.; Saikku, L.; Kauppi, P.E. Carbon gains and recovery from degradation of forest biomass in European Union during 1990–2005. *Forest Ecol. Manage.* **2010**, *259*, 1232–1238.

10. Pan, Y.D.; Birdsey, R.A.; Fang, J.Y.; Houghton, R.; Kauppi, P.E.; Kurz, W.A.; Phillips, O.L.; Shvidenko, A.; Lewis, S.L.; Canadell, J.G.; *et al.* A large and persistent carbon sink in the world's forests. *Science* **2011**, *333*, 988–993.

11. Goetz, S.; Dubayah, R. Advances in remote sensing technology and implications for measuring and monitoring forest carbon stocks and change. *Carbon Manage.* **2011**, *2*, 231–244.

12. Kauppi, P.E. New, low estimate for carbon stock in global forest vegetation based on inventory data. *Silva Fenn.* **2003**, *37*, 451–457.

13. Kauppi, P.E.; Ausubel, J.H.; Fang, J.Y.; Mather, A.S.; Sedjo, R.A.; Waggoner, P.E. Returning forests analyzed with the forest identity. *Proc. Natl. Acad. Sci. USA* **2006**, *103*, 17574–17579.

14. Lefsky, M.A. A global forest canopy height map from the Moderate Resolution Imaging Spectroradiometer and the Geoscience Laser Altimeter System. *Geophys. Res. Lett.* **2010**, *37*, doi: 10.1029/2010gl043622.

15. Simard, M.; Pinto, N.; Fisher, J.B.; Baccini, A. Mapping forest canopy height globally with spaceborne lidar. *J. Geophys. Res-Biogeosci.* **2011**, *116*, doi: 10.1029/2011jg001708.

16. Saatchi, S.S.; Harris, N.L.; Brown, S.; Lefsky, M.; Mitchard, E.T.A.; Salas, W.; Zutta, B.R.; Buermann, W.; Lewis, S.L.; Hagen, S.; *et al.* Benchmark map of forest carbon stocks in tropical regions across three continents. *Proc. Natl. Acad. Sci. USA* **2011**, *108*, 9899–9904.

17. Kempes, C.P.; West, G.B.; Crowell, K.; Girvan, M. Predicting maximum tree heights and other traits from allometric scaling and resource limitations. *Plos One* **2011**, *6*, doi: 10.1371/journal.pone.0020551.

18. Jung, S.-E.; Kwak, D.-A.; Park, T.; Lee, W.-K.; Yoo, S. Estimating crown variables of individual trees using airborne and terrestrial laser scanners. *Remote Sens.* **2011**, *3*, 2346–2363.

19. Straub, C.; Koch, B. Estimating single tree stem volume of *Pinus sylvestris* using airborne laser scanner and multispectral line scanner data. *Remote Sens.* **2011**, *3*, 929–944.

20. Treuhaft, R.N.; Chapman, B.D.; dos Santos, J.R.; Goncalves, F.G.; Dutra, L.V.; Graca, P.M.L.A.; Drake, J.B. Vegetation profiles in tropical forests from multibaseline interferometric synthetic aperture radar, field, and lidar measurements. *J. Geophys. Res-Atmos.* **2009**, *114*, doi: 10.1029/ 2008jd011674.

21. Treuhaft, R.N.; Goncalves, F.G.; Drake, J.B.; Chapman, B.D.; dos Santos, J.R.; Dutra, L.V.; Graca, P.M.L.A.; Purcell, G.H. Biomass estimation in a tropical wet forest using Fourier transforms of profiles from lidar or interferometric SAR. *Geophys. Res. Lett.* **2010**, *37*, doi: 10.1029/2010gl045608.

22. Baccini, A.; Goetz, S.J.; Walker, W.S.; Laporte, N.T.; Sun, M.; Sulla-Menashe, D.; Hackler, J.; Beck, P.S.A.; Dubayah, R.; Friedl, M.A.; *et al.* Estimated carbon dioxide emissions from tropical deforestation improved by carbon-density maps. *Nature Clim. Change* **2012**, *2*, 182–185.

23. Zhang, G.; Ganguly, S.; Nemani, R.; White, M.; Milesi, C.; Wang, W.; Saatchi, S.; Yu, Y.; Myneni, R.B. A simple parametric estimation of live forest aboveground biomass in California using satellite derived metrics of canopy height and Leaf Area Index. *Geophys. Res. Lett.* **2013**, under review.

24. Lefsky, M.A.; Harding, D.J.; Keller, M.; Cohen, W.B.; Carabajal, C.C.; Espirito-Santo, F.D.; Hunter, M.O.; de Oliveira, R. Estimates of forest canopy height and aboveground biomass using ICESat. *Geophys. Res. Lett.* **2005**, *32*, doi: 10.1029/2005gl023971.

25. Lefsky, M.A.; Keller, M.; Pang, Y.; de Camargo, P.B.; Hunter, M.O. Revised method for forest canopy height estimation from Geoscience Laser Altimeter System waveforms. *J. Appl. Remote Sens.* **2007**, *1*, doi: 10.1117/1.2795724.

26. Moorcroft, P.R.; Hurtt, G.C.; Pacala, S.W. A method for scaling vegetation dynamics: The ecosystem demography model (ED). *Ecol. Monogr.* **2001**, *71*, 557–585.

27. Shi, Y.; Choi, S.; Ni, S.; Ganguly, S.; Zhang, G.; Duong, H.V.; Lefsky, M.A.; Simard, M.; Saatchi, S.S.; Lee, S.; *et al.* Allometric scaling and resource limitations model of tree heights: Part 1. Model optimization and testing over continental USA. *Remote Sens.* **2013**, under review.

28. Powell, M.J.D. An efficient method for finding the minimum of a function of several variables without calculating derivatives. *Computer J.* **1964**, *7*, 155–162.

29. Condit, R. The CTFS and the Standardization of Methodology. In *Tropical Forest Census Plots: Methods and Results from Barro Colorado Island, Panama, and a Comparison with Other Plots*; Chapter 1.1; Springer: Berlin/Germany; New York, NY, USA, 1998; pp. 3–8.

30. Hubbell, S.P.; Foster, R.B.; O'Brien, S.T.; Harms, K.E.; Condit, R.; Wechsler, B.; Wright, S.J.; de Lao, S.L. Light-gap disturbances, recruitment limitation, and tree diversity in a neotropical forest. *Science* **1999**, *283*, 554–557.

31. Hubbell, S.P.; Condit, R.; Foster, R.B. *Barro Colorado Forest Census Plot Data*. Center for Tropical Forest Science of Smithsonian Tropical Research Institute, Panama, Republic of Panama, 2005. Available online: https://ctfs.arnarb.harvard.edu/webatlas/datasets/bci (accessed on 15 April 2012).

32. *Penobscot Experimental Forest.* Available online: http://www.fs.fed.us/ne/durham/4155/ penobsco.htm (accessed on 15 April 2012).

33. Cook, B.; Dubayah, R.; Hall, F.; Nelson, R.; Ranson, J.; Strahler, A.; Siqueira, P.; Simard, M.; Griffith, P. *NACP New England and Sierra National Forests Biophysical Measurements: 2008–2010*; Oak Ridge National Laboratory Distributed Active Archive Center: Oak Ridge, TN, USA, 2011. Available online: http://dx.doi.org/10.3334/ORNLDAAC/1046 (accessed on 15 April 2012).

34. Strahler, A.H.; Schaaf, C.; Woodcock, C.; Jupp, D.; Culvenor, D.; Newnham, G.; Dubayah, R.; Yao, T.; Zhao, F.; Yang, X. *ECHIDNA Lidar Campaigns: Forest Canopy Imagery and Field Data, U.S.A., 2007–2009*; Oak Ridge National Laboratory Distributed Active Archive Center: Oak Ridge, TN, USA, 2011. Available online: http://dx.doi.org/10.3334/ORNLDAAC/1045 (accessed on 15 April 2012).

35. *ECHIDNA Lidar Campaigns: Forest Canopy Imagery and Field Data, USA, 2007–2009.* Available online: http://daac.ornl.gov//NACP/guides/ECHIDNA.html (accessed on 15 April 2012).

36. Blair, J.B.; Rabine, D.L.; Hofton, M.A. The Laser vegetation imaging sensor: A medium-altitude, digitisation-only, airborne laser altimeter for mapping vegetation and topography. *ISPRS J. Photogramm.* **1999**, *54*, 115–122.

37. Lee, S.; Ni-Meister, W.; Yang, W.Z.; Chen, Q. Physically based vertical vegetation structure retrieval from ICESat data: Validation using LVIS in White Mountain National Forest, New Hampshire, USA. *Remote Sens. Environ.* **2011**, *115*, 2776–2785.

38. *Laser Vegetation Imaging Sensor.* Available online: https://lvis.gsfc.nasa.gov/index.php (accessed on 15 April 2012).

39. Geoscience Laser Altimeter System. Available online: http://nsidc.org/daac/projects/lidar/glas.html (accessed on 15 April 2012).

40. Zwally, H.J.; Schutz, B.; Abdalati, W.; Abshire, J.; Bentley, C.; Brenner, A.; Bufton, J.; Dezio, J.; Hancock, D.; Harding, D.; *et al.* ICESat's laser measurements of polar ice, atmosphere, ocean, and land. *J. Geodyn.* **2002**, *34*, 405–445.

41. Abshire, J.B.; Sun, X.L.; Riris, H.; Sirota, J.M.; McGarry, J.F.; Palm, S.; Yi, D.H.; Liiva, P. Geoscience Laser Altimeter System (GLAS) on the ICESat mission: On-orbit measurement performance. *Geophys. Res. Lett.* **2005**, *32*, doi: 10.1029/2005gl024028.

42. Gong, P.; Li, Z.; Huang, H.B.; Sun, G.Q.; Wang, L. ICESat GLAS data for urban environment monitoring. *IEEE Trans. Geosci. Remote Sens.* **2011**, *49*, 1158–1172.

43. Baldocchi, D.; Falge, E.; Gu, L.H.; Olson, R.; Hollinger, D.; Running, S.; Anthoni, P.; Bernhofer, C.; Davis, K.; Evans, R.; *et al.* FLUXNET: A new tool to study the temporal and spatial variability of ecosystem-scale carbon dioxide, water vapor, and energy flux densities. *Bull. Amer. Meteor. Soc.* **2001**, *82*, 2415–2434.

44. *DAYMET.* Available online: http://www.daymet.org/ (accessed on 15 April 2012).

45. *Guide to Meteorological Instruments and Methods of Observation, Appendix 4B, WMO-No. 8 (CIMO Guide)*, 7th ed.; World Meteorological Organization (WMO): Geneva, Switzerland, 2008.

46. Masek, J.G.; Vermote, E.F.; Saleous, N.E.; Wolfe, R.; Hall, F.G.; Huemmrich, K.F.; Gao, F.; Kutler, J.; Lim, T.K. A Landsat surface reflectance dataset for North America, 1990–2000. *IEEE Geosci. Remote Sens.* **2006**, *3*, 68–72.

47. Ganguly, S.; Nemani, R.R.; Zhang, G.; Hashimoto, H.; Milesi, C.; Michaelis, A.; Wang, W.; Votava, P.; Samanta, A.; Melton, F.; *et al.* Generating global Leaf Area Index from Landsat: Algorithm formulation and demonstration. *Remote Sens. Environ.* **2012**, *122*, 185–202.

48. Lovell, J.L.; Jupp, D.L.B.; Culvenor, D.S.; Coops, N.C. Using airborne and ground-based ranging lidar to measure canopy structure in Australian forests. *Can. J. Remote Sens.* **2003**, *29*, 607–622.

49. Anderson, J.; Martin, M.E.; Smith, M.L.; Dubayah, R.O.; Hofton, M.A.; Hyde, P.; Peterson, B.E.; Blair, J.B.; Knox, R.G. The use of waveform lidar to measure northern temperate mixed conifer and deciduous forest structure in New Hampshire. *Remote Sens. Environ.* **2006**, *105*, 248–261.

50. Anderson, J.E.; Plourde, L.C.; Martin, M.E.; Braswell, B.H.; Smith, M.L.; Dubayah, R.O.; Hofton, M.A.; Blair, J.B. Integrating waveform lidar with hyperspectral imagery for inventory of a northern temperate forest. *Remote Sens. Environ.* **2008**, *112*, 1856–1870.

51. Ballhorn, U.; Jubanski, J.; Siegert, F. ICESat/GLAS data as a measurement tool for peatland topography and peat swamp forest biomass in Kalimantan, Indonesia. *Remote Sens.* **2011**, *3*, 1957–1982.

52. Rosette, J.A.B.; North, P.R.J.; Suarez, J.C.; Los, S.O. Uncertainty within satellite LiDAR estimations of vegetation and topography. *Int. J. Remote Sens.* **2010**, *31*, 1325–1342.

53. Pflugmacher, D.; Cohen, W.; Kennedy, R.; Lefsky, M. Regional applicability of forest height and aboveground biomass models for the Geoscience Laser Altimeter System. *Forest Sci.* **2008**, *54*, 647–657.

54. Neuenschwander, A.L. Evaluation of waveform deconvolution and decomposition retrieval algorithms for ICESat/GLAS data. *Can. J. Remote Sens.* **2008**, *34*, S240-S246.

55. Chen, Q. Retrieving vegetation height of forests and woodlands over mountainous areas in the Pacific Coast region using satellite laser altimetry. *Remote Sens. Environ.* **2010**, *114*, 1610–1627.

56. Sun, G.; Ranson, K.J.; Kimes, D.S.; Blair, J.B.; Kovacs, K. Forest vertical structure from GLAS: An evaluation using LVIS and SRTM data. *Remote Sens. Environ.* **2008**, *112*, 107–117.

57. Harding, D.J.; Carabajal, C.C. ICESat waveform measurements of within-footprint topographic relief and vegetation vertical structure. *Geophys. Res. Lett.* **2005**, *32*, doi: 10.1029/2005gl023471.

58. Pang, Y.; Lefsky, M.; Sun, G.Q.; Ranson, J. Impact of footprint diameter and off-nadir pointing on the precision of canopy height estimates from spaceborne lidar. *Remote Sens. Environ.* **2011**, *115*, 2798–2809.

59. Duncanson, L.I.; Niemann, K.O.; Wulder, M.A. Estimating forest canopy height and terrain relief from GLAS waveform metrics. *Remote Sens. Environ.* **2010**, *114*, 138–154.

60. Wang, K.; Franklin, S.E.; Guo, X.L.; Cattet, M. Remote sensing of ecology, biodiversity and conservation: A review from the perspective of remote sensing specialists. *Sensors* **2010**, *10*, 9647–9667.

61. Press, W.H.; Teukolsky, S.A.; Vetterling, W.T.; Flannery, B.P. Minimization or Maximization of Functions. In *Numerical Recipes in FORTRAN: The Art of Scientific Computing*, 2nd ed.; Chapter 10; Cambridge University Press: Cambridge, NY, USA, 1992; pp. 394–455.

62. Kuusk, A.; Nilson, T. A directional multispectral forest reflectance model. *Remote Sens. Environ.* **2000**, *72*, 244–252.

63. TRY. *Plant Trait Database*. Available online: http://www.try-db.org/TryWeb/Home.php (accessed on 12 July 2012).

64. Gholz, H.L. Environmental limits on aboveground net primary production, leaf area, and biomass in vegetation zones of the Pacific Northwest. *Ecology* **1982**, *63*, 469–481.

65. Smith, T.M.; Shugart, H.H.; Bonan, G.B.; Smith, J.B. Modeling the potential response of vegetation to global climate change. *Adv. Ecol. Res.* **1992**, *22*, 93–116.

66. Ridler, M.E.; Sandholt, I.; Butts, M.; Lerer, S.; Mougin, E.; Timouk, F.; Kergoat, L.; Madsen, H. Calibrating a soil–vegetation–atmosphere transfer model with remote sensing estimates of surface temperature and soil surface moisture in a semi arid environment. *J. Hydrol.* **2012**, *436–437*, 1–12.

67. Shugart, H.H.; Saatchi, S.; Hall, F.G. Importance of structure and its measurement in quantifying function of forest ecosystems. *J. Geophys. Res-Biogeosci.* **2010**, *115*, doi: 10.1029/2009jg000993.

68. Obrien, S.T.; Hubbell, S.P.; Spiro, P.; Condit, R.; Foster, R.B. Diameter, height, crown, and age relationships in 8 neotropical tree species. *Ecology* **1995**, *76*, 1926–1939.

69. Halfon, E. Probabilistic validation of computer-simulations using the bootstrap. *Ecol. Model.* **1989**, *46*, 213–219.

70. Pan, Y.; Chen, J.M.; Birdsey, R.; McCullough, K.; He, L.; Deng, F. Age structure and disturbance legacy of North American forests. *Biogeosciences* **2011**, *8*, 715–732.

71. Dubayah, R.O.; Sheldon, S.L.; Clark, D.B.; Hofton, M.A.; Blair, J.B.; Hurtt, G.C.; Chazdon, R.L. Estimation of tropical forest height and biomass dynamics using lidar remote sensing at La Selva, Costa Rica. *J. Geophys. Res-Biogeosci.* **2010**, *115*, doi 10.1029/2009jg000933.

72. Fricker, G.A.; Saatchi, S.S.; Meyer, V.; Gillespie, T.W.; Sheng, Y.W. Application of semi-automated filter to improve waveform Lidar sub-canopy elevation model. *Remote Sens.* **2012**, *4*, 1494–1518.

73. Holdridge, L.R.; Tosi, J.A. The Life Zone. In *Life Zone Ecology*; Chapter 2; Tropical Science Center: San Jose, Costa Rica, 1967; pp. 7–18.

74. Pandey, G.R.; Cayan, D.R.; Dettinger, M.D.; Georgakakos, K.P. A hybrid orographic plus statistical model for downscaling daily precipitation in northern California. *J. Hydrometeorol.* **2000**, *1*, 491–506.

75. Lundquist, J.D.; Cayan, D.R. Surface temperature patterns in complex terrain: Daily variations and long-term change in the central Sierra Nevada, California. *J. Geophys. Res-Atmos.* **2007**, *112*, doi: 10.1029/2006jd007561.